Published in final edited form as:
Nat Biotechnol. 2009 January ; 27(1): 59–65. doi:10.1038/nbt.1515.

Intravascular AAV9 preferentially targets neonatal-neurons and adult-astrocytes in CNS

Kevin D. Foust[1], **Emily Nurre**[1,2], **Chrystal L. Montgomery**[1], **Anna Hernandez**[3], **Curtis M. Chan**[3], and **Brian K. Kaspar**[1,2]

[1]Center for Gene Therapy, The Research Institute at Nationwide Children's Hospital, 700 Children's Drive, Columbus, Ohio, 43205

[2]Department of Pediatrics, College of Medicine, The Ohio State University, Columbus, OH, 43205

[3]Special Pathology Services, Charles River, Preclinical Services Nevada, Reno, NV, 89511

Abstract

Delivery of therapeutics to the brain and spinal cord remains a challenge for neurodegenerative diseases, such as spinal muscular atrophy (SMA) and amyotrophic lateral sclerosis (ALS). The blood-brain-barrier (BBB) hampers delivery of therapeutics to neurons, glia, and surrounding cell types of the central nervous system (CNS) that may be involved in disease progression. Here, we describe an intravenous injection of adeno-associated-virus-9 (AAV-9) in mouse that efficiently targets brain, dorsal root ganglia and spinal cord motor neurons in neonatal animals and astrocytes in adult mouse brain and spinal cords, offering a new therapeutic delivery approach to deliver genes to widespread regions within the CNS.

Introduction

To date, approximately 100% of large-molecule drugs do not cross the BBB and 98% of small-molecules cannot penetrate this barrier, thereby limiting drug development efforts for many CNS disorders[1]. Gene delivery has recently been proposed as a method to bypass the BBB[2]; however, widespread delivery to the brain and spinal cord has been challenging. The development of successful gene therapies for motor neuron disease will likely require widespread transduction within the spinal cord and motor cortex. Two of the most common motor neuron diseases are SMA and ALS, both debilitating disorders of children and adults, respectively, with no effective therapies to date. Recent work in rodent models of SMA and ALS have demonstrated significant promise for gene delivery using viruses that are retrogradely transported following intramuscular injection, and is currently being explored for clinical trials[2–5]. However, clinical development may be difficult given the numerous injections required to target the widespread region of neurodegeneration throughout the spinal cord, brainstem and motor cortex to effectively treat these diseases. AAV vectors have shown significant promise in a number of recent clinical trials for neurological disorders, demonstrating sustained transgene expression, a relatively safe profile, and promising functional responses, yet have required surgical intraparenchymal injections[6–8].

Advances in delivery of newly discovered AAV serotypes-6, −8, and −9 have demonstrated remarkable widespread transduction throughout multiple tissues such as skeletal and cardiac

Correspondence should be addressed to: Brian K. Kaspar, Ph.D. The Research Institute at Nationwide Children's Hospital The Ohio State University 700 Children's Drive, WA3022 Columbus, OH 43205 Ph: 614.722.5085 Fax: 614.355.5247 Brian.Kaspar@NationwideChildrens.org.

muscles following simple systemic intravenous or intraperitoneal injections[9–13]. These serotypes have all been shown to cross vascular endothelial cell barriers efficiently. However, the use of a vascular delivery approach to target lower motor neurons or other cell types within the CNS has been inefficient, likely due to the inability of the virus to cross the blood-brain-barrier (BBB). AAV serotypes −6 and −8 showed poor penetration of the CNS following vascular gene delivery in neonate- or adult-animals, only expressing in several cells within the spinal cord[14, 15]. We therefore investigated the behavior of a new AAV serotype-9 which also crosses vascular endothelium, but has unique serological characteristics from previously described serotypes[16], to efficiently deliver genes to the CNS via intravenous delivery in both neonate animals, where the BBB is not fully developed, and in adult mice, where the BBB is fully formed.

Results

Intravenous injection of AAV9 in neonates predominantly targets motor neurons in spinal cord

To evaluate lower motor neuron transduction (LMN), our first studies investigated transgene expression following intravenous injection in neonate animals, prior to the closure of the BBB. One-day-old wild-type mice received temporal vein injections of 4×10^{11} particles of a self-complementary (sc) AAV9 vector[17] that expressed green fluorescent protein (GFP) under control of the chicken-β-actin hybrid promoter (CB). Animals were sacrificed 10-or 21-days post-injection, and brains and spinal cords were evaluated for transgene expression. Robust GFP-expression was found in heart and skeletal muscles as expected (data not shown). Strikingly, spinal cords had remarkable GFP-expression throughout all levels, with robust GFP-expression in fibers that ascended in the dorsal columns and fibers that innervated the spinal grey matter, indicating dorsal root ganglia (DRG) transduction. GFP-positive cells were also found in the ventral region of the spinal cord where lower motor neurons reside (Fig. 1a, d, e and h). Co-labeling for choline acetyl transferase (ChAT) and GFP-expression within the spinal cord demonstrated a large number of ChAT positive cells expressing GFP throughout all cervical and lumbar sections examined, indicating widespread LMN transduction (Fig. 1l, Supplementary Fig. 1 online). Approximately 56% of ChAT positive cells strongly expressed GFP in sections analyzed of the lumbar spinal cord of 10 day-old animals and ~61% of 21 day-old animals, demonstrating early and persistent transgene expression in lower motor neurons (Table 1). Similar numbers of LMN expression were seen in cervical and thoracic regions of the spinal cord. To our knowledge, this is the highest proportion of LMNs transduced by a single injection of AAV reported. In addition to widespread DRG and motor neuron transduction, we observed GFP-positive glial cells throughout the spinal grey matter, indicating that AAV9 could express in astrocytes with the CB promoter (Fig. 1l). *In situ* hybridization performed with riboprobes against the viral construct on frozen spinal cord tissue confirmed that viral transcription, and not protein uptake, was responsible for the previously unseen transduction pattern (Fig. 2).

Intravenous injection of AAV9 in neonates targets neurons and astrocytes in brain

We next examined the brains following postnatal day-one intravenous injection of scAAV9-CB-GFP and found extensive GFP-expression in all regions analyzed, including the striatum, cortex, anterior commissure, internal capsule, corpus callosum, hippocampus and dentate gyrus, midbrain and cerebellum (Fig. 3a–h, respectively, Fig. 4a–d). GFP-positive cells included both neurons and astrocytes throughout the brain. To further characterize the transduced neurons, brains were co-labeled for GFP and GAD67, a GABAergic marker. The cortex, hippocampus and dentate had very little co-localization between GFP and GAD67 labeled cells (Supplementary Fig. 2a–i online), while Purkinje cells in the cerebellum were extensively co-labeled (Supplementary Fig. 2j–l online). Finally, unbiased-estimated

stereological quantification of transduction showed that 15 +/−0.9% within the retrosplenial/cingulate cortex, 11 +/− 0.5% within the dentate gyrus and 64 +/−8.2% within the Purkinje layer of total neurons were transduced 10-days post-injection. The percent of transduced neurons increased to 18 +/−1.9% within the retrosplenial/cingulate cortex, 14 +/− 4.8% within the dentate gyrus, and 71 +/−3.0% within the Purkinje layer 21-days following a one-time administration of virus (Table 1). The increased numbers at 21-days post-injection were likely due to an increase in gene expression detected. However the differences detected 10- or 21-days post-injection were not statistically different ($p>0.05$), demonstrating stable transgene expression over time.

Mode of Viral Entry into the CNS

The remarkable pattern of GFP-expression observed following postnatal day-one administration suggests two independent modes of viral entry into the CNS. Due to the ubiquitous GFP-expression throughout the brain, the virus likely crossed the developing BBB. However the GFP-expression pattern in the neonate spinal cord is defined with respect to the specific DRG and LMN transduction. The DRG and the LMN have projections into the periphery which suggests retrograde transport may be the mechanism of transduction. In support of retrograde transport as the method of spinal cord neuronal transduction, there were no GFP-positive interneurons observed in any section examined (Fig. 1d,h). Alternatively, the virus may have a LMN tropism after crossing the BBB, but this appears unlikely as ChAT positive cells still migrating from the central canal to the ventral horn were largely untransduced (Fig. 1d,h). Given this finding, we hypothesized that AAV9 may have a property of enhanced retrograde transport, to target DRG and LMNs at high efficiency. To investigate whether AAV9 vectors were enhanced for retrograde transport, we tested the ability for AAV9 to be retrogradely transported in adult animals. Direct intramuscular injection of AAV9 into adult gastrocnemius muscles led to high gene expression in myofibers, yet we did not readily detect GFP-expression in motor neurons. These results suggest that AAV9 vectors do not possess enhanced transport properties, at least when tested in adult mice (Supplementary Fig. 3 online). However, this result did not exclude the potential for AAV9 to target DRG and LMNs in the adult following systemic delivery.

Widespread targeting of astrocytes in the spinal cord following vascular delivered AAV9

We next injected adult mice via tail vein delivery with doses ranging from 4×10^{11} to 4×10^{12} particles of scAAV9-CB-GFP. GFP-expression was found in heart and skeletal muscles as expected (data not shown). In contrast to neonates, we found a strikingly different transduction pattern in adult-treated animals. Most noticeably, there was an absence of GFP-positive DRG fibers and a marked decrease in LMN transduction in all cervical and lumbar spinal cord sections examined. Interestingly, GFP-positive astrocytes were easily observed throughout the entire dorsal-ventral extent of the grey matter in all regions of the spinal cord (Fig. 5a–h) with the greatest GFP-expression levels found in the higher dosed animals. Co-labeling of GFP-positive cells with astroglial markers excitatory amino acid transporter 2 (EAAT2) and glial fibrillary acidic protein (GFAP) demonstrated that approximately 90% of the GFP-positive cells were astrocytes. Counts of total astroctyes in the lumbar region of the spinal cord by z-series collected confocal microscopy showed over 64% of total astrocytes were positive for GFP (Fig. 5i–l, Table 1). To date, predominant glial transduction has not been reported for any AAV serotype following intravenous delivery indicating that AAV9 has a unique transduction property in the adult CNS when delivered intravenously. In our analysis, we did note an occasional motor neuron transduced in the spinal cord, although these events were scarce in adult animals. Viral transcription was again confirmed in adult tissues with *in situ* hybridization (Fig. 2). Furthermore, whereas neonate intravenous injection resulted in indiscriminate astrocyte and neuronal transduction throughout the brain,

adult tail-vein injections produced isolated and localized neuronal expression only in the hippocampus and dentate gyrus (Fig. 4e–f, Fig. 5m–n), in both low and high dose animals. Low-dose animals had isolated patches of transduced astrocytes scattered throughout the entire brain (data not shown). Of significance, high-dose animals had extensive astrocyte and vascular transduction throughout the entire brain (Fig. 4e–f, Fig. 5m–p) that persisted for at least seven-weeks post-injection (n=5), suggesting a dose-response of transduction, without regional specificity.

Predominant astrocyte transduction in adults is injection route dependent

Interestingly, the pattern of transduction shifted, from primarily neuronal targeting in neonate-, to astrocytic targeting in adult-treated animals. To date, our results demonstrate the greatest efficiency for targeting astrocytes in rodents. However, a recent manuscript reported efficient astrocyte transduction by an AAV8-, but not an AAV9-vector, following direct brain injection[18]. Astrocyte transduction, however, was suggested to be related to viral purification[18]. To investigate whether astrocyte transduction was related to vector purity or delivery route in our study, we evaluated multiple AAV9 preparations for vector purity by silver-stain and injected 8×10^{10} particles of the same scAAV9-CB-GFP vector preparations from the intravenous experiments into the striatum and dentate gyrus of adult mice. Silver-staining showed that vector preparations were relatively pure and of research grade quality (Supplementary Fig. 4 online). Two-weeks post-intracranial injection, we observed significant neuronal transduction within the injected regions using these vector preparations. However, we found no evidence for co-localization between GFP and GFAP labeling throughout the injected brains (n=3) (Supplementary Fig. 5 online), as previously reported[19], suggesting the astrocyte transduction in our study may be injection route and serotype dependent and not due to vector purity.

Discussion

The findings presented in this study demonstrate a unique capacity for AAV9-vectors to cross the BBB in varying degrees given the timepoint of gene administration. The delivery of AAV9-GFP in the neonate resulted in widespread neuronal targeting with an apparent tropism towards motor neurons residing within the spinal cord. Within numerous regions of the brain, we found substantial transduction of neurons. Interestingly, based upon our data, GABAergic interneurons were not highly transduced by AAV9 using a vascular delivery approach, yet pyramidal and Purkinje neurons were highly transduced. These transduced cells have long projection axons, unlike interneurons. Our results may postulate that the specific neuroanatomy, such as neuronal morphology or vascular density may determine the capacity of which neurons are transduced by AAV9 in this injection paradigm. These results justify further study which may provide insight into the mechanisms for viral gene transfer of AAV9-based vectors to specific neuronal populations.

The scarcity of LMN and DRG transduction seen in the adult paradigm suggests there is a developmental period in which access by circulating virus to these cell populations becomes restricted. Assuming a dependence on retrograde transport for DRG and LMN transduction following intravenous injection, Schwann cell or synapse maturation may be an important determinant of successful AAV9 LMN and DRG transduction. Previously, we reported retrograde transport by AAV vectors[20, 21] and recently some serotypes have demonstrated an increased capability for retrograde transport[22]. However, we did not detect obvious retrograde transport from AAV9 vectors following intramuscular injection in adult treated animals.

The predominant astrocyte transduction in adults suggests that AAV9 escapes brain vasculature in a similar manner as skeletal and cardiac muscle vasculature. The ability for

AAV9 to penetrate or bypass endothelium is of interest. Normally, tight junctions severely restrict BBB penetration of molecules, such as viruses. AAV9 may be utilizing transport proteins, receptor mediated transcytosis, adsorptive transcytosis or other mechanisms to gain access across the BBB. Once free of the vasculature, our data suggests that AAV9 infects the astrocytic-perivascular-endfeet that surround capillary endothelial cells[23]. Our results highlight the interesting aspect that astrocytes are targeted only when the virus is exposed to the astrocytic perivascular-endfeet. Given that astrocytes retain some features of apical-basal polarity from development, certain receptors or channels may be accessible via this vascular entry route compared to direct intraparencymal injections[24]. The precise mechanism of bypassing endothelial cells leading to astrocytic transduction will require further study.

In summary, our results demonstrate the unique capacity of AAV9 to efficiently target cells within the CNS, and in particular, widespread neuronal and motor neuron transduction in the neonate, and extensive astrocyte transduction in the adult following intravenous delivery. A simple intravenous injection of AAV9 as we describe here may be clinically relevant for both SMA and ALS. In the context of SMA, data suggests that increased expression of survival motor neuron (*SMN*) gene in LMNs may hold therapeutic benefit[3, 25]. The importance of the results presented here is that with a single injection we may be able to effectively restore *SMN* expression levels in LMNs. Additionally, given the robust neuronal populations transduced throughout the CNS in neonatal animals, this approach may also allow for rapid, relatively inexpensive generation of chimeric animals for gene overexpression, or gene knock-down[26]. Additionally, constructing AAV9 based vectors with neuronal or astrocyte specific promoters may allow further specificity, given that AAV9 targets multiple non-neuronal tissues following intravenous delivery[11, 13]. Our results also demonstrated efficient targeting of astrocytes in adult-treated animals, and this finding may be relevant for treating ALS, where the non-cell autonomous nature of disease progression has recently been discovered, and astrocytes have been specifically linked to disease progression[27]. The ability to target astrocytes for producing trophic factors, or to circumvent aberrant glial activity may be beneficial for treating ALS[28]. Noteworthy, AAV9 vascular delivery in the adult does not achieve widespread direct neuronal targeting, limiting this approach for diseases such as Huntington's where multiple structures and brain regions likely require neuronal targeting to suppress mutant Huntington[29, 30]. However, the ability to generate viruses that are more efficient and reach neurons in the adult by vascular delivery may be possible with newly generated techniques in viral evolution based on AAV9 capsids[31–33]. In sum, our results highlight a relatively non-invasive method to efficiently deliver genes to the CNS and may be useful in basic and clinical neurology studies.

Methods

Virus

AAV9 was produced by transient transfection procedures using a double stranded AAV2-ITR based CB-GFP vector, with a plasmid encoding Rep2Cap9 sequence as previously described[16] along with a adenoviral helper plasmid; pHelper (Stratagene, La Jolla, CA) in 293 cells. Our serotype 9 sequence was verified by sequencing and identical to that previously described[16]. Virus was produced in 3 separate batches for the experiments by a contract manufacturing company (Virapur LLC, San Diego, CA) and purified by two cesium chloride density gradiet purification steps, dialyzed against phosphate-buffered-saline (PBS) and formulated with 0.001% Pluronic-F68 to prevent virus aggregation and stored at 4°C. All vector preparations were titered by quantitative-PCR using Taq-Man technology. Purity of vectors was assessed by 4–12% SDS-Acrylamide gel electrophoresis and silver staining (Invitrogen, Carlsbad, CA).

Animals

Mice used were C57Bl/6 littermates. The mother (singly housed) of each litter to be injected was removed from the cage. The postnatal day-1 pups were rested on a bed of ice for anesthetization. For neonate injections, a light microscope was used to visualize the temporal vein (located just anterior to the ear). Vector solution was drawn into a 3/10cc 30 gauge insulin syringe. The needle was inserted into the vein and the plunger was manually depressed. Virus injections were in a total volume of 100μl of a phosphate buffered saline (PBS) supplemented with 0.001% Pluronic-F68. A total of 4×10^{11} DNase resistant particles of scAAV9-CB-GFP (Virapur LLC, San Diego, CA) were injected. A correct injection was verified by noting blanching of the vein. After the injection, pups were returned to their cage. When the entire litter was injected, the pups were rubbed with bedding to prevent rejection by the mother. The mother was then reintroduced to the cage. Neonate animals were sacrificed ten- or twenty-one-days post injection, spinal cords and brains were extracted, rinsed in PBS, then immersion fixed in a 4% paraformaldehyde solution.

Adult tail vein injections were performed on ~70 day old C57Bl/6 mice. Mice were placed in restraint that positioned the mouse tail in a lighted, heated groove. The tail was swabbed with alcohol then injected intravenously with a 100 μl viral solution containing a mixture of PBS and 4×10^{11}, 8×10^{11} or 4×10^{12} DNase resistant particles of scAAV9-CB-GFP. After the injection, animals were returned to their cages. Two- to seven-weeks post-injection, animals were anesthetized then transcardially perfused first with 0.9% saline, then 4% paraformaldehyde. Brains and spinal cords were harvested and immersion fixed in 4% paraformaldehyde for an additional 24–48 hours.

Adult intramuscular injections were performed on ~75 day old C57Bl/6 mice as previously described[34]. Mice were anesthetized with isoflurane, and a small incision was made over the right gastrocnemius muscle. A 50μl viral solution containing 5×10^{10} particles of scAAV9 CB GFP was injected over three sites in the gastrocnemius with a 3/10cc 30 gauge insulin syringe. The incision was closed and the animals were allowed to recover.

Histological processing

Neonate and adult brains were transferred from paraformaldehyde to a 30% sucrose solution for cryoprotection. The brains were mounted onto a sliding microtome with Tissue-Tek O.C.T. compound (Sakura Finetek USA, Torrance, CA) and frozen with dry ice. Forty micron thick sections were divided into 5 series for histological analysis. Tissues for immediate processing were placed in 0.01 M PBS in vials. Those for storage were placed in antifreeze solution and transferred to −20°C. Spinal cords were cut into blocks of tissue 5–6mm in length, and then cut into 40 micron thick transverse sections on a vibratome (Leica, Bannockburn, IL). Serial sections were kept in a 96-well plate that contained 4% paraformaldehyde and were stored at 4°C.

Muscles were dissected, snap-frozen in liquid nitrogen-cooled isopentane, cryostat sectioned, and mounted onto slides for observation of GFP fluorescence.

Immunohistochemistry

Brains and spinal cords were both stained as floating sections. Brains were stained in a 12-well dish, and spinal cords sections were stained in a 96-well plate to maintain their rostral-caudal sequence. Tissues were washed three-times for 5-minutes each in PBS, then blocked in a solution containing 10% donkey serum and 1% Triton X-100 for two hours at room temperature. After blocking, antibodies were diluted in the blocking solution at 1:500. The primary antibodies used were as follows: goat anti-ChAT and mouse anti-NeuN (Millipore, Billerica, MA), rabbit anti-GFP (Invitrogen, Carlsbad, CA), guinea pig anti-GFAP

(Advanced Immunochemical, Long Beach, CA) and goat anti-GAD67 (Millipore, Billerica, MA). Tissues were incubated in primary antibody at 4°C for 48–72 hours then washed three times with PBS. After washing, tissues were incubated for 2 hours at room temperature in the appropriate secondary antibodies (1:125 Jackson Immunoresearch, Westgrove, PA) with DAPI. Tissues were then washed three times with PBS, mounted onto slides then coverslipped. All images were captured on a Zeiss-laser-scanning confocal microscope.

In Situ Hybridization

Using a plasmid which contained T3- and T7-promoter sequences with a cloned GFP gene, we performed PCR to generate antisense and sense DIG-UTP labeled GFP riboprobes. Probe yield and incorporation of DIG-UTP was confirmed by electrophoresis and dot blot. 10μm-thick sections of spinal cord mounted on SuperFrost slides were prepared by fixation with 4% paraformaldehyde, washed in 0.5× SSC, permeabilized by incubation in Proteinase K (2.5μg/ml), washed in 0.5× SSC and dehydrated in series of alcohol washes. Pre-hybridization was performed at 42 °C using RiboHybe buffer (Ventana, Tucson, AZ) for 1-hour followed by hybridization overnight at 55 °C with the respective riboprobes on AAV9-injected and PBS-control-injected neonatal and adult cord sections. Stringency washes were performed and immunological detection using anti-Digoxigenin AP antibody (1:500, Roche, Palo Alto, CA) and development with NBT/BCIP (Pierce, Rockford, IL) and Nuclear Fast Red (Vector, Burlingame, CA).

Stereology and Motor neuron and astrocyte quantification

Stereology for total number of neurons in a given area and total number of GFP+ cells was performed on a Nikon E800 fluorescent microscope with computer-assisted microscopy and image analysis using StereoInvestigator software (MicroBrightField, Inc., Williston, VT) with the optical dissector principle to avoid oversampling errors and the Cavalieri estimation for volumetric measurements. Coronal 40μm sections, 240μm apart covering the regions of interest in its rostro-caudal extension was evaluated. The entire dentate gyrus, caudal retrosplenial/cingulate cortex; containing the most caudal extent of the dentate gyrus; extending medially to the subiculum and laterally to the occipital cortex, and the Purkinje cell layer was sampled using ~15–25 optical dissectors in each case. Fluorescent microscopy using a 60× objective for NeuN and GFP were utilized and cells within the optical dissector were counted on a computer screen. Neuronal density and positive GFP density were calculated by multiplying the total volume to estimate the percent of neuronal transduction in each given area as previously described[35]. The volume of the granule cell layer was 1.76 × 108 +/− 0.11 × 108 μm^3 and 1.95 ×108 +/− .17 μm^3. The sample volume was 9,000 μm^3. The Purkinje cell layer volume was 3870 μm^3 +/− 195 μm^3 for 10-day and 4135 μm^3 +/− 98 μm^3. The coefficient of error for the cell counts ranged from 0.05 to 0.10. Statistical analysis showed no differences between 10- and 21-days post-injection for any structure analyzed.

For motor neuron quantification, serial 40μm thick lumbar spinal cord sections, each separated by 480 μm, were labeled as described for GFP and ChAT expression. Stained sections were serially mounted on slides from rostral to caudal, then coverslipped. Sections were evaluated using confocal microscopy (Zeiss) with a 40× objective and simultaneous FITC and Cy3 filters. FITC was visualized through a 505–530nm band pass filter to avoid contaminating the Cy3 channel. The total number of ChAT positive cells found in the ventral horns with defined soma was tallied by careful examination through the entire z-extent of the section. GFP labeled cells were quantified in the same manner, while checking for co-localization with ChAT. The total number of cells counted per animal ranged from approximately 150–366 cells per animal. For astrocyte quantification, as with motor neurons, serial sections were stained for GFP, GFAP and EAAT2, then mounted. Using confocal microscopy with a 63× objective and simultaneous FITC and Cy5 filters, random

fields in the ventral horns of lumbar spinal cord sections from tail vein injected animals were selected. The total numbers of GFP and GFAP positive cells were counted from a minimum of at least 24-fields per animal while focusing through the entire z extent of the section.

Statistical Analysis

Statistical analyses were performed using Graph Pad Prizm software (San Diego, CA). Means were represented with standard error of means (s.e.m.). Student-t-tests were performed to compare 10- versus 21-days post-injection using a 95% confidence level.

Supplementary Material

Refer to Web version on PubMed Central for supplementary material.

Acknowledgments

This work was supported by NIH/NEI R21EY018491, NIH/NINDS R21NS064328, Project A.L.S. and The Muscular Dystrophy Association. We kindly thank Jeff Rothstein (Johns Hopkins University) for the EAAT2 antibody, Terri Shaffer (Nationwide Children's Hospital) for expertise in mouse tail vein injections, and Michele Basso (Ohio State University) and Megan Detloff (Ohio State University) for stereology usage and advice.

References

1. Pardridge WM. Drug and gene targeting to the brain with molecular Trojan horses. Nat Rev Drug Discov 2002;1:131–139. [PubMed: 12120094]
2. Kaspar BK, Llado J, Sherkat N, Rothstein JD, Gage FH. Retrograde viral delivery of IGF-1 prolongs survival in a mouse ALS model. Science 2003;301:839–842. [PubMed: 12907804]
3. Azzouz M, et al. Lentivector-mediated SMN replacement in a mouse model of spinal muscular atrophy. J Clin Invest 2004;114:1726–1731. [PubMed: 15599397]
4. Azzouz M, et al. VEGF delivery with retrogradely transported lentivector prolongs survival in a mouse ALS model. Nature 2004;429:413–417. [PubMed: 15164063]
5. Ralph GS, et al. Silencing mutant SOD1 using RNAi protects against neurodegeneration and extends survival in an ALS model. Nat Med 2005;11:429–433. [PubMed: 15768029]
6. Kaplitt MG, et al. Safety and tolerability of gene therapy with an adeno-associated virus (AAV) borne GAD gene for Parkinson's disease: an open label, phase I trial. Lancet 2007;369:2097–2105. [PubMed: 17586305]
7. Marks WJ Jr. et al. Safety and tolerability of intraputaminal delivery of CERE-120 (adeno-associated virus serotype 2-neurturin) to patients with idiopathic Parkinson's disease: an open-label, phase I trial. Lancet Neurol 2008;7:400–408. [PubMed: 18387850]
8. Worgall S, et al. Treatment of Late Infantile Neuronal Ceroid Lipofuscinosis by CNS Administration of a Serotype 2 Adeno-Associated Virus Expressing CLN2 cDNA. Hum Gene Ther. 2008
9. Blankinship MJ, et al. Efficient transduction of skeletal muscle using vectors based on adeno-associated virus serotype 6. Mol Ther 2004;10:671–678. [PubMed: 15451451]
10. Wang Z, et al. Adeno-associated virus serotype 8 efficiently delivers genes to muscle and heart. Nat Biotechnol 2005;23:321–328. [PubMed: 15735640]
11. Inagaki K, et al. Robust systemic transduction with AAV9 vectors in mice: efficient global cardiac gene transfer superior to that of AAV8. Mol Ther 2006;14:45–53. [PubMed: 16713360]
12. Nakai H, et al. Unrestricted hepatocyte transduction with adeno-associated virus serotype 8 vectors in mice. J Virol 2005;79:214–224. [PubMed: 15596817]
13. Pacak CA, et al. Recombinant adeno-associated virus serotype 9 leads to preferential cardiac transduction in vivo. Circulation research 2006;99:e3–9. [PubMed: 16873720]
14. Towne C, Raoul C, Schneider BL, Aebischer P. Systemic AAV6 delivery mediating RNA interference against SOD1: neuromuscular transduction does not alter disease progression in fALS mice. Mol Ther 2008;16:1018–1025. [PubMed: 18414477]

15. Foust KD, Poirier A, Pacak CA, Mandel RJ, Flotte TR. Neonatal intraperitoneal or intravenous injections of recombinant adeno-associated virus type 8 transduce dorsal root ganglia and lower motor neurons. Hum Gene Ther 2008;19:61–70. [PubMed: 18052722]
16. Gao G, et al. Clades of Adeno-associated viruses are widely disseminated in human tissues. J Virol 2004;78:6381–6388. [PubMed: 15163731]
17. McCarty DM, et al. Adeno-associated virus terminal repeat (TR) mutant generates self-complementary vectors to overcome the rate-limiting step to transduction in vivo. Gene Ther 2003;10:2112–2118. [PubMed: 14625565]
18. Klein RL, Dayton RD, Tatom JB, Henderson KM, Henning PP. AAV8, 9, Rh10, Rh43 vector gene transfer in the rat brain: effects of serotype, promoter and purification method. Mol Ther 2008;16:89–96. [PubMed: 17955025]
19. Cearley CN, et al. Expanded repertoire of AAV vector serotypes mediate unique patterns of transduction in mouse brain. Mol Ther 2008;16:1710–1718. [PubMed: 18714307]
20. Kaspar BK, et al. Targeted retrograde gene delivery for neuronal protection. Mol Ther 2002;5:50–56. [PubMed: 11786045]
21. Miller TM, et al. Gene transfer demonstrates that muscle is not a primary target for non-cell-autonomous toxicity in familial amyotrophic lateral sclerosis. Proceedings of the National Academy of Sciences of the United States of America 2006;103:19546–19551. [PubMed: 17164329]
22. Hollis ER 2nd, Kadoya K, Hirsch M, Samulski RJ, Tuszynski MH. Efficient retrograde neuronal transduction utilizing self-complementary AAV1. Mol Ther 2008;16:296–301. [PubMed: 18223548]
23. Abbott NJ, Ronnback L, Hansson E. Astrocyte-endothelial interactions at the blood-brain barrier. Nat Rev Neurosci 2006;7:41–53. [PubMed: 16371949]
24. Abbott NJ. Dynamics of CNS barriers: evolution, differentiation, and modulation. Cellular and molecular neurobiology 2005;25:5–23. [PubMed: 15962506]
25. Baughan T, et al. Stimulating full-length SMN2 expression by delivering bifunctional RNAs via a viral vector. Mol Ther 2006;14:54–62. [PubMed: 16580882]
26. Siegel RM, Callaway EM. Francis Crick's legacy for neuroscience: between the alpha and the Omega. PLoS Biol 2004;2:e419. [PubMed: 17593891]
27. Yamanaka K, et al. Astrocytes as determinants of disease progression in inherited amyotrophic lateral sclerosis. Nat Neurosci 2008;11:251–253. [PubMed: 18246065]
28. Dodge JC, et al. Delivery of AAV-IGF-1 to the CNS Extends Survival in ALS Mice Through Modification of Aberrant Glial Cell Activity. Mol Ther. 2008
29. Harper SQ, et al. RNA interference improves motor and neuropathological abnormalities in a Huntington's disease mouse model. Proceedings of the National Academy of Sciences of the United States of America 2005;102:5820–5825. [PubMed: 15811941]
30. Rodriguez-Lebron E, Denovan-Wright EM, Nash K, Lewin AS, Mandel RJ. Intrastriatal rAAV-mediated delivery of anti-huntingtin shRNAs induces partial reversal of disease progression in R6/1 Huntington's disease transgenic mice. Mol Ther 2005;12:618–633. [PubMed: 16019264]
31. Maheshri N, Koerber JT, Kaspar BK, Schaffer DV. Directed evolution of adeno-associated virus yields enhanced gene delivery vectors. Nat Biotechnol 2006;24:198–204. [PubMed: 16429148]
32. Li W, et al. Engineering and selection of shuffled AAV genomes: a new strategy for producing targeted biological nanoparticles. Mol Ther 2008;16:1252–1260. [PubMed: 18500254]
33. Koerber JT, Jang JH, Schaffer DV. DNA shuffling of adeno-associated virus yields functionally diverse viral progeny. Mol Ther 2008;16:1703–1709. [PubMed: 18728640]
34. Haidet AM, et al. Long-term enhancement of skeletal muscle mass and strength by single gene administration of myostatin inhibitors. Proceedings of the National Academy of Sciences of the United States of America 2008;105:4318–4322. [PubMed: 18334646]
35. Kempermann G, Kuhn HG, Gage FH. Genetic influence on neurogenesis in the dentate gyrus of adult mice. Proceedings of the National Academy of Sciences of the United States of America 1997;94:10409–10414. [PubMed: 9294224]

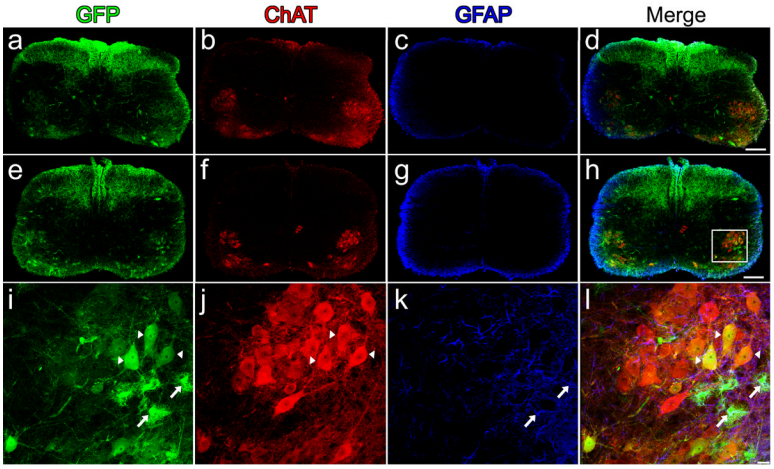

Figure 1.

Intravenous injection of AAV9 leads to widespread neonatal spinal cord transduction. Cervical (**a–d**) and lumbar (**e–l**) spinal cord sections ten-days following facial-vein injection of 4×10^{11} particles of scAAV9-CB-GFP into postnatal day-1 mice (*n*=8). GFP-expression (**a,e,i**) was predominantly restricted to lower motor neurons (**a,e,i**) and fibers that originated from dorsal root ganglia (**a,e**). GFP-positive astrocytes (**i,l, arrows**) were also observed scattered throughout the tissue sections. Lower motor neuron and astrocyte expression were confirmed by co-localization using choline acetyl transferase (ChAT) (**b, f,j**) and glial fibrillary acidic protein (GFAP) (**c,g,k**), respectively. Merged images of GFP, ChAT and GFAP (**d,h,l**). A z-stack image (**i–l**) of the area within the box in **h**, shows the extent of motor neuron (arrow heads) and astrocyte (arrows) transduction within the lumbar spinal cord. Scale bars, 200 μm (**d,h**), 20 μm (**l**).

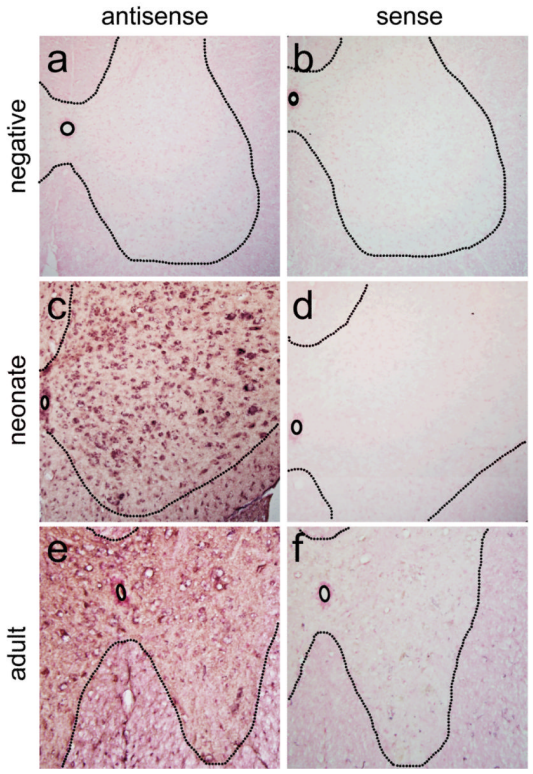

Figure 2.

In situ hybridization of spinal cord sections from neonate and adult injected animals demonstrates that cells expressing GFP are transduced with scAAV9-CB-GFP. Negative control animals injected with PBS (**a–b**) showed no positive signal (*n*=2). However, antisense probes for GFP demonstrated strong positive signals for both neonate (*n*=3) (**c**) and adult (*n*=3) (**e**) sections analyzed. No positive signals were found for the sense control probe in neonate (**d**) or adult (**f**) spinal cord sections. Tissues were counterstained with Nuclear Fast Red for contrast while probe hybridization is in purple.

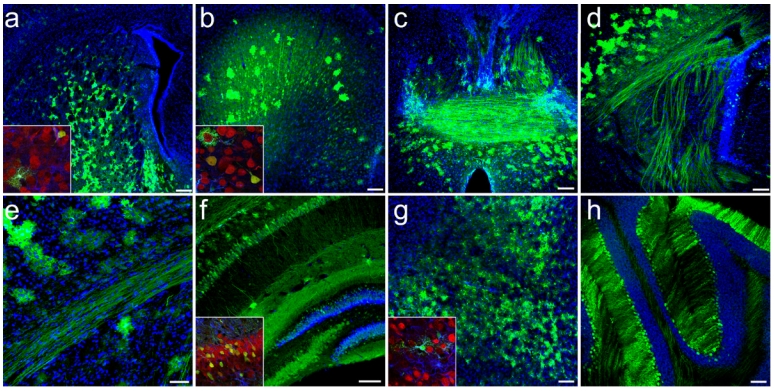

Figure 3.

Widespread GFP-expression 21-days following intravenous injection of 4×10^{11} particles of scAAV9-CB-GFP to postnatal day-1 mice. GFP localized in neurons and astrocytes throughout multiple structures of the brain (*n*=6) as depicted in: (**a**) striatum (**b**) cingulate gyrus (**c**) fornix and anterior commissure (**d**) internal capsule (**e**) corpus callosum (**f**) hippocampus and dentate gyrus (**g**) midbrain and (**h**) cerebellum. All large panels show GFP (green) and dapi (blue) merged images. Insets of selected regions show high magnification merged images of GFP (green), NeuN (red) and GFAP (blue) labeling. Schematic representations depicting the approximate locations of each image throughout the brain are shown in (Supplementary Fig. 6). Higher magnification images of select structures are available in (Fig. 4). Scale bars, 200 μm (**a**); 50 μm (**e**); 100 μm (**b–d,f–h**)

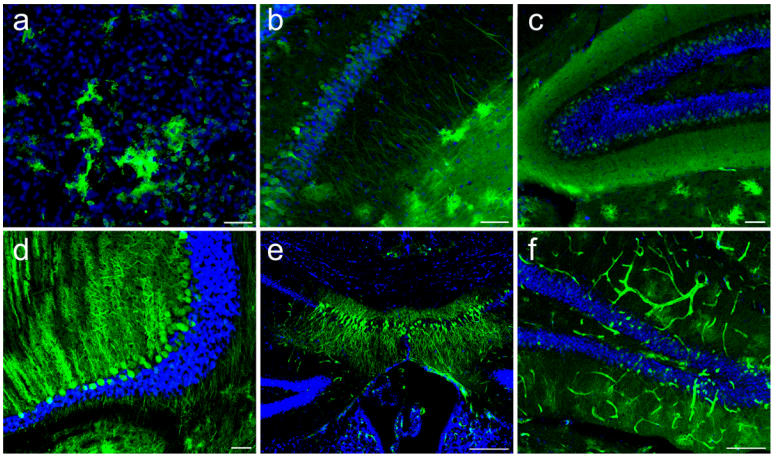

Figure 4.

High-magnification of merged GFP (green) and dapi (blue) images of brain regions following neonate (*n*=8) (**a–d**) or adult (*n*=6) (**e–f**) intravenous injection of scAAV9-CB-GFP. Astrocytes and neurons were easily detected in the striatum (**a**), hippocampus (**b**) and dentate gyrus (**c**) following postnatal day-1 intravenous injection of 4×10^{11} particles of scAAV9-CB-GFP. Extensive GFP-expression within cerebellar Purkinje cells (**d**) was also observed. Pyramidal cells of the hippocampus (**e**) and granular cells of the dentate gyrus (**f**) were the only neuronal transduction within the brain following adult tail vein injection. In addition to astrocyte and neuronal transduction, widespread vascular transduction (**f**) was also seen throughout all adult brain sections examined. Scale bars, 200μm (**e**); 100μm (**f**), 50μm (**a–d**)

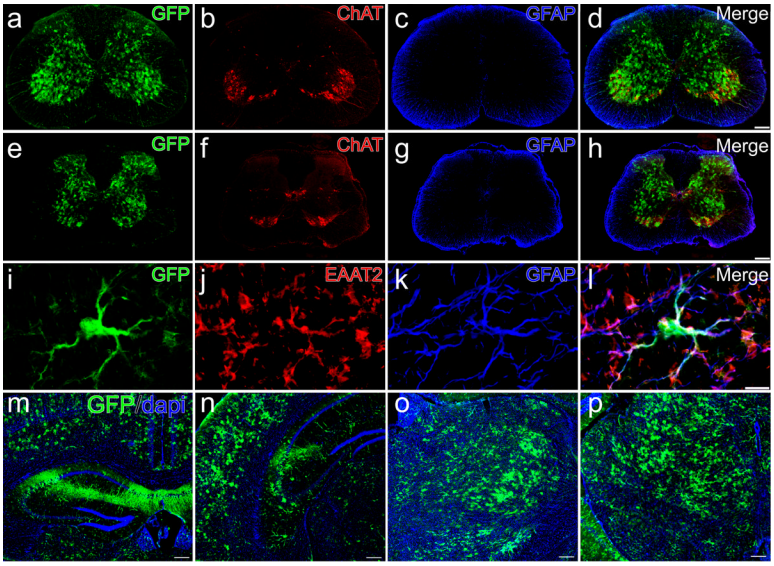

Figure 5.

Intravenous injection of AAV9 leads to widespread predominant astrocyte transduction in the spinal cord and brain of adult mice. GFP-expression in the cervical (**a–d**) and lumbar (**e–h**) spinal cord as well as the brain (**m–p**) of adult mice 7-weeks after tail vein injection of 4×10^{12} particles of scAAV9-CB-GFP (*n*=6). In contrast to postnatal day-1 intravenous injections, adult tail vein injection resulted in almost exclusively astrocyte transduction. GFP (**a,e**), ChAT (**b,f**) and GFAP (**c,g**) demonstrate the abundance of GFP-expression throughout the spinal grey matter, with lack of co-localization with lower motor neurons and white matter astrocytes (**d,h**). Co-localization of GFP (**i**), excitatory amino acid transporter 2 (EAAT2) (**j**), and GFAP (**k**) confirm that transduced cells are astrocytes (**l**). Tail vein injection also resulted in primarily astrocyte transduction throughout the brain as seen in the cortex (**m–n**), thalamus (**o**) and midbrain (**p**). All brain panels show GFP (green) and dapi (blue) merged images. Neuronal GFP-expression in the brain was restricted to the hippocampus and dentate gyrus (**m–n**, Fig. 4 e–f). Schematic representations depicting the approximate locations of each image throughout the brain are available in. (Supplementary Fig. 7) Scale bars, 10 μm (**l**),200 μm (**d,h,p**)

Table 1

		Neonate		
		GFP (mean+/− s.e.m.)	NeuN (mean +/− s.e.m.)	% (mean +/− s.e.m.)
Brain	**Retrosplenial/Cingulate**			
	10-days post-injection	108,232 +/− 6,677	684,909 +/− 15,293	15 +/− 0.9
	21-days post-injection	142,658 +/− 11,124	762,104 +/− 38,397	18+/− 1.9
	Dentate Gyrus			
	10-days post-injection	26,978 +/− 2,568	228,184 +/− 21,835	11 +/− 0.5
	21-days post-injection	42,304 +/− 15,613	278,043 +/− 11,383	14 +/− 4.8
	Purkinje cells			
	10-days post-injection	46,505 +/− 8,885	71,740 +/− 6,049	64 +/− 8.2
	21-days post-injection	52,720 +/− 1,951	73,814 +/− 5,220	71 +/− 3.0

		GFP (mean +/− s.e.m.)	ChAT (mean +/− s.e.m.)	% (mean +/− s.e.m.)
Lumbar spinal cord	10-days post-injection	149 +/− 31	264 +/− 53	56 +/− 1.9
	21-days post-injection	83 +/− 16	140 +/− 31	60 +/− 2.9

		Adult		
		GFP (mean +/− s.e.m.)	GFAP (mean +/− s.e.m.)	% (mean +/− s.e.m.)
Lumbar spinal cord (grey matter)	% GFP colabeled w/ GFAP	48 +/− 10	43 +/− 7	91 +/− 4.8
	% GFAP+ transduced	41 +/− 5	64 +/− 8	64 +/− 0.9